RSC Advances

PAPER

View Article Online
View Journal | View Issue

Cite this: *RSC Adv.*, 2023, **13**, 9099

Magnetocaloric effect and Griffiths phase analysis in a nanocrystalline Ho_2NiMnO_6 and Ho_2CoMnO_6 double perovskite

K. P. Shinde,[a] C. Hwang,[a] M. Manawan,[b] Y.-S. Choi,[c] S.-Y. Park,[c] Y. Jo,[c] S. Lee,[a] D.-H. Kim*[d] and J. S. Park *[a]

Received 10th January 2023
Accepted 11th March 2023

DOI: 10.1039/d3ra00199g

rsc.li/rsc-advances

Rare-earth double perovskite oxides have intriguing magnetocaloric properties at cryogenic temperatures. In this study, Ho_2NiMnO_6 and Ho_2CoMnO_6 were synthesized using the sol–gel method, which crystallized in a monoclinic structure in the $P2_1/n$ space group. The magnetic phase transition was observed at 81.2 K for Ho_2NiMnO_6 and 73.5 K for Ho_2CoMnO_6. The presence of a paramagnetic matrix and short-range ferromagnetic clusters causes magnetic disorder in these double perovskites, resulting in Griffiths phase formation. The Arrott plot confirms that compounds undergo second-order phase transition. At an applied magnetic field of 5 T, the maximum magnetic entropy change ($-\Delta S$) for the studied compounds is 1.7 and 2.2 J kg^{-1} K^{-1}, respectively. The transition metals Ni and Co in a double perovskite cause lattice distortion in the structural parameters and oxidation states of manganese (Mn^{3+}/Mn^{4+}), which changes the magnetic and magnetocaloric properties. The quantitative approach provides a systematic study of magnetocaloric properties of the rare earth double perovskite compounds with ferromagnetic 3d transition elements.

1. Introduction

Magnetic refrigeration is a cooling technology based on the magnetocaloric effect (MCE), which has recently attracted much attention because of its high conversion efficiency and environmental friendliness.[1–4] The MCE is defined as the magneto-thermal response of a magnetic material arising due to the coupling of the magnetic sublattice with the external magnetic field. The temperature of MCE materials increases or decreases when we apply or remove the magnetic field.[5] So far, numerous magnetocaloric materials have been explored for possible applications in magnetic refrigeration (MR) at a wide range of temperatures from ambient to liquid He temperature. The various materials with a substantial MCE at low temperatures, such as rare-earth based alloys,[6–8] rare-earth amorphous alloys,[9,10] rare earth oxides,[11,12] and double perovskites[13–18] have been extensively investigated over the years. Among them, magnetic oxides are a class of materials that are being explored for their potential applications in magnetic refrigeration technology, due to their high resistivity and low eddy current loss. They are also attractive for fundamental studies, as they are simple to prepare and chemically stable.[19,20] However, in the literature it was reported that the adiabatic temperature change of magnetic oxides is limited by their relatively high heat capacity.[21]

On the other hand, the rare-earth based double perovskite (DP) compounds having the general formula $A_2B'B''O_6$ (A = rare earth metal, B′ = di-valent transition metal, B″ = tri-valent transition metal, O = oxygen) are discovered to have a variety of remarkable properties, including ferroelectricity, half-metallic transport, piezoelectricity, magnetic ordering, and a large MCE.[22–24] By carefully selecting and combining the constituent ions, it is possible to realize various exciting properties based on changes in the ionic radii and electronic configurations of B′ and B ions.[25] Among the double perovskite families, R_2MMnO_6 (R = rare earth element, M = Ni, Co) has recently attracted substantial interest due to its controllability of magnetic and electronic properties.[26,27] These DP compounds contain Co^{2+} ions with electronic configuration d^7 tse_g^2 and Mn^{4+} with electronic configuration d^3 t_2g^3 e_g^0, which exhibit ferromagnetic ordering due to Co^{2+} and Mn^{4+} superexchange interactions.[28,29] These types of DP compounds are mostly ferromagnetic and insulating, with the formation of ferromagnetic cluster. The evolution of a Griffiths-like phase is observed in the paramagnetic region for some cases. Due to the antisite disorder in this type of DP, antiferromagnetic ordering has also been observed at lower temperatures. In some compounds,

[a]*Department of Materials Science and Engineering, Hanbat National University, Daejeon 34158, South Korea. E-mail: jsphb@hanbat.ac.kr*

[b]*Fakultas Teknologi Pertahanan, Universitas Pertahanan Indonesia, Bogor 16810, Indonesia*

[c]*Center for Scientific Instrumentation, Korea Basic Science Institute, Daejeon 34133, South Korea*

[d]*Department of Physics, Chungbuk National University, Cheongju 28644, South Korea. E-mail: donghyun@chungbuk.ac.kr*

anti-parallel ordering of Co^{2+}/Mn^{4+} and R^{3+} spins have also been observed, resulting in antiferromagnetic state at low temperature. Among the various rare-earth based DP materials, $Ho_2B'B''O_6$ is relatively less studied compound.[13,15,17,22] However holmium, with its high magnetic moment and smaller ionic radius compared to other rare-earth elements, could be an intriguing element for A-site in determining structural and magnetic properties of DP materials system.

It is known that non-Ho DP compounds, such as Gd_2NiMnO_6 and Gd_2CoMnO_6 exhibits significant MCE at low temperatures, with $-\Delta S$ values of 35.5 J kg^{-1} K^{-1} and 24 J kg^{-1} K^{-1}, respectively, for H = 0–7 T.[30] In a study by Zhang *et al.*[31] cryogenic magnetic properties and magnetocaloric effect in Pr_2NiMnO_6 and Pr_2CoMnO_6 compounds, reporting the second-order phase transition with $-\Delta S$ values of 3.15 at 208 K and 3.91 J kg^{-1} K^{-1} at 170 K under an applied field of 7 T. In our previous work,[32] we reported that the varying the B-site in double perovskite materials prepared by solid-state reaction with different transition metal elements results in variation of Curie temperature. Li *et al.*[33] recently published a study on the effect of B′-site ordering on magnetocaloric and critical behavior in Nd_2BMnO_6 with B = Ni and Co. It should be mentioned that the preparation conditions highly influence the microstructure of the DP materials, with determination of related physical properties of DP materials.[34] Recently, magnetocaloric properties in distorted double perovskite due to different ionic radius of rare earth elements in RE_2NiTiO_6 have been reported. It was found that in case of Gd_2NiTiO_6 compound MCE properties are better than other two compounds.[35] The transition temperature and magnetocaloric effect can be enhanced by substituting non-magnetic Ti^{3+} ion in $Gd_2CoMnTiO_6$ compound by Zheng *et al.*[36] It was found that MCE enhanced from 16.64 J kg^{-1} K^{-1} to 27.16 J kg^{-1} K^{-1} under ΔH = 6 T at cryogenic temperature. Patra *et al.*[37] reported the synthesis of Ho_2CoMnO_6 nanorod by using hydrothermal route and magnetocaloric effect gives a change in entropy value of 12.4 J kg^{-1} K^{-1} at low temperature for 7 T.

Here, we report the fabrication of nanocrystalline Ho_2NiMnO_6 and Ho_2CoMnO_6 compounds using the sol–gel method. The structural, magnetic, and magnetocaloric behavior have been systematically investigated, where the Griffiths phase (GP) behavior and first-/second-order phase transition behavior are intensively explored.

2. Experimental

Double perovskite Ho_2NiMnO_6 (HNMO) and Ho_2CoMnO_6 (HCMO) were synthesized using the sol–gel method. The stoichiometric amounts of high purity $Ni(NO_3)_2\cdot 6H_2O$, $Co(NO_3)_2\cdot 6H_2O$, and $Mn(NO_3)_2\cdot xH_2O$ from Sigma Aldrich were dissolved in distilled water. The trivalent rare earth Ho_2O_3 oxide was dissolved in concentrated nitric acid along with few drops of oxalic acid. In the metallic salt mixture, an appropriate amount of citric acid and ethylene glycol is added, and the solution pH is maintained to 8 using ammonia. The final mixture was kept on the hot plate at 80 °C with constant stirring for 4 h to get a homogeneous gel. The temperature of hot plate was increased to 100 °C to burn the gel to get the final product in the form of powder. The resulting powders were grounded mechanically and sintered at 1200 °C for 48 h. The phase purity of the prepared compounds and crystal structures were confirmed using powder X-ray diffraction (PXRD) with Cu-Kα radiation at room temperature by using the Bruker D8 Advance diffractometer. The high-resolution transmission electron microscopy (HRTEM) studies were carried out with a HITACHI HF 5000 electron microscope. The magnetic properties were measured by using the Magnetic Properties Measurement System (MPMS, Quantum design). The temperature-dependent magnetization curve was measured in FC (field cooling) and ZFC (zero field cooling) mode at an applied magnetic field (H = 100 Oe, 500 Oe, 1000 Oe, and 10 000 Oe) in a temperature range of 2–200 K. The temperature dependence of magnetization isotherms were recorded with 3 K steps in the 0–5 T range around the Curie temperature (T_C) for each compound to estimate magnetic entropy change.

3. Results and discussion

The X-ray diffraction (XRD) patterns for Ho_2NiMnO_6 (HNMO) and Ho_2CoMnO_6 (HCMO) powder compounds are illustrated in Fig. 1(a and b). The crystallographic information of the present compounds has been extracted by Rietveld refinement using the Topas software and structural analysis software VESTA.[38,39] The XRD analysis confirms that the HNMO and HCMO compounds crystallize in a monoclinic structure with space group $P2_1/n$. The refinement parameters such as R_{exp}, R_{WP}, GoF, lattice constant, volume, bond angle, and bond length for both compounds are summarized in Table 1. It is confirmed that determined parameters are in good agreement with the literature.[40,41] The peak located at $2\theta = 29.2°$ corresponds to the impurity phase of Ho_2O_3, and the impurity phase contributions are approximately 10.35 and 7.63 wt% for HNMO and HCMO, respectively. NiO weak impurity phase is observed as well in case of HNMO compound. The impurity phases of rare-earth oxides exist particularly in DP compounds prepared by sol–gel method as reported by Zhang *et al.*[42] Inset of Fig. 1 shows the three-dimensional atomic arrangement of the monoclinic structure of HNMO and HCMO. The octahedral structure of CoO_6/NiO_6 and MnO_6 are shared in such a way to form the alternate layer in a unit cell of double perovskite as seen in the figure. The octahedron tilt angle and the perovskite structure stability change with the difference in the radius of the A and B/B′ metal ions in double perovskite.[43] To confirm the presence of the double perovskite structure and the degree of distortion from the ideal cubic structure, we have calculated the Goldschmidt tolerance factor given by the following formula.

$$t = \frac{r_O + r_A}{\sqrt{2}\left[r_O + \frac{(r_B + r_{B'})}{2}\right]} \quad (1)$$

where the r_A, r_B, and $r_{B'}$ are the ionic radii of A, B, B′, and O ions, respectively. The t values of HNMO and HCMO determined by using the eqn (1) are 0.869 and 0.878, respectively. The tolerance factor less than 1 indicates that the ionic radius of A-site cation in DP is smaller, which causes stress in structure,

correspondingly resulting in the change in the bond length or octahedral tilting.[44]

Fig. 2(a and b) shows the transmission electron microscope images for HNMO and HCMO compounds. The particles size and shape are not uniform due to high-temperature sintering process. From these images, the nanocrystalline nature of prepared DP compounds is confirmed to have a particle size of about 50–200 nm. The selected area electron diffraction (SAED) pattern for HNMO and HCMO compounds shown in Fig. 2(c and d), exhibits ordered spot diffraction patterns with bright spots at regular positions, evidencing their nanocrystalline nature.

The temperature-dependent magnetization was measured in zero-field cooled (ZFC) and field cooled (FC) mode as shown in Fig. 3(a and b) for the HNMO and HCMO at different magnetic fields of $H = 100$, 500, 1000, and 10 000 Oe. In ZFC mode sample was cooled down in the absence of a magnetic field from 300 K to 2 K, and measurement was taken in heating, while in FC mode, the magnetic field was applied, the sample was cooled from 300 K to 2 K, and measurement was taken in heating. The behavior of M–T plots indicates the paramagnetic (PM) to the ferromagnetic (FM) phase transition at the Curie-temperature (T_C) which can be determined precisely from the first derivative of the magnetization curve (dM/dT). The determined values of T_C are 81 K and 73 K for HNMO and HCMO, respectively, and slightly lower than the reported values in the literature.[16,22] The observed divergence between the FC and ZFC curves in HNMO and HCMO was like previous reports on double perovskite compounds, which is considered to be due to the magnetic frustration present in the compounds at a low magnetic field. This magnetic frustration occurs due to the mixed oxidation states of the Mn^{3+}/Mn^{4+} cations present in the compound. As we increase an applied magnetic field, divergence in ZFC and FC is reduced due to the spin reorientation process, reducing, in turn, the magnetic frustrations present in the compounds. It is evident that the magnetic susceptibility in the paramagnetic phase follows the Curie–Weiss law, the magnetic susceptibility $\chi = \frac{C}{T-\theta}$, where C represents the Curie constant and θ is the Curie–Weiss temperature. The inset of Fig. 3(a and b) shows the temperature dependence of inverse magnetic susceptibility with Curie–Weiss fitting. The experimental value of effective moment in paramagnetic region allows us to calculate μ_{eff}^{exp} in the unit of Bohr magneton by using the following equation:[45]

$$\mu_{eff}^{exp}(\mu_B) = \left(\frac{3Ck_B}{N_a{\mu_B}^2}\right)^{1/2} = \sqrt{8C} \quad (2)$$

where N_a and k_B represent Avogadro number and Boltzmann constant, respectively. The estimated value of experimental paramagnetic moment was found to be 15.0 and 15.4 μ_B/f.u for HNMO and HCMO, respectively. The calculated effective magnetic moments are in good agreement with the theoretically calculated values given by using the following equation:[46]

Table 1 List of parameters obtained from Rietveld refinement of HNMO and HCMO powder XRD pattern and tolerance parameter

	Ho_2NiMnO_6	Ho_2CoMnO_6
Space group	$P2_1/n$	$P2_1/n$
Cell mass (g mol^{-1})	1078.98	1079.46
Cell volume (Å^3)	215.13	214.37
Crystal density (g cm^{-3})	8.33	8.36
Lattice parameters		
a (Å)	5.2102	5.2016
b (Å)	5.5293	5.5370
c (Å)	7.4677	7.4431
β (°)	90.115	89.981
Bond angle (°)		
M–O_1–Mn	147.6	147.5
M–O_2–Mn	145.3	145.2
M–O_3–Mn	149.7	149.5
Av. bond length (Å)		
M–O	1.99	2.07
R_{exp} (%)	1.10	0.77
R_{wp} (%)	3.98	2.38
GoF	3.61	3.11
t	0.869	0.878
μ_{eff} (μ_B) cal.	15.00	15.41
μ_{eff} (μ_B) theo.	15.73	15.95

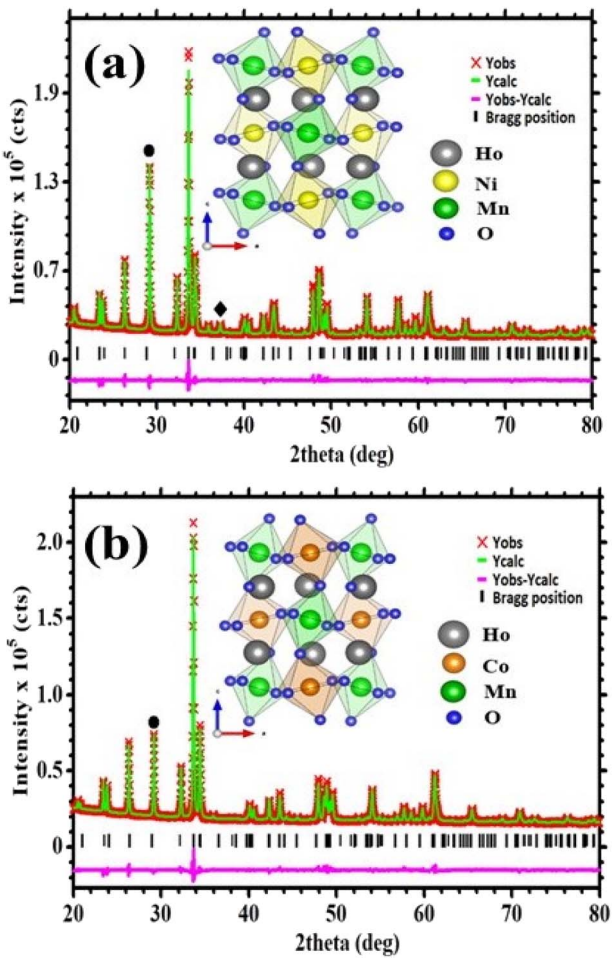

Fig. 1 Room temperature XRD patterns with Rietveld refinement analysis for (a) Ho_2NiMnO_6 (b) Ho_2CoMnO_6. Insets: crystal structure of corresponding compounds.

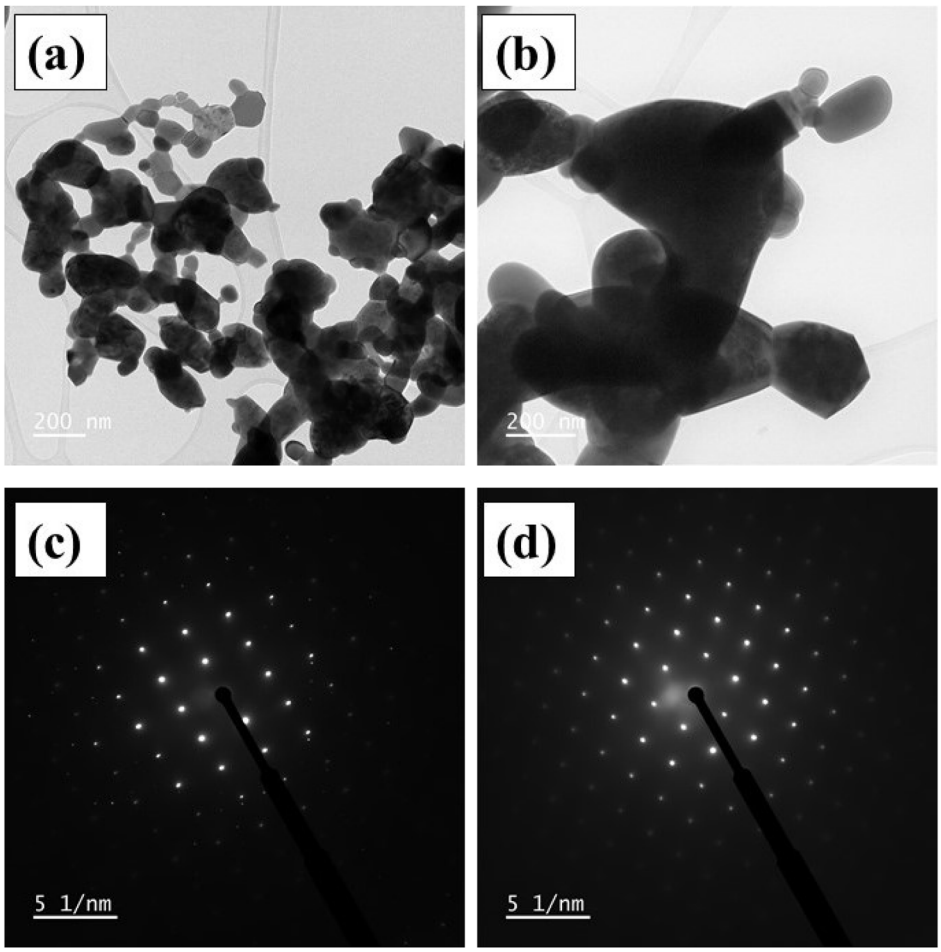

Fig. 2 (a and b) Transmission electron microscope images (c and d) selected area electron diffraction (SAED) patterns of HNMO and HCMO compounds.

$$\mu_{\text{eff}}^{\text{exp}}(\mu_B) = \sqrt{2 \times \mu_{\text{eff}}{}^2(Ho^{3+}) + \mu_{\text{eff}}{}^2(Ni^{2+}) + \mu_{\text{eff}}{}^2(Mn^{4+})} \quad (3)$$

where the effective paramagnetic moments for $\mu_{\text{eff}}(Ho^{3+}) = 10.6$ μ_B, $\mu_{\text{eff}}(Ni^{2+}) = 2.83$ μ_B, $\mu_{\text{eff}}(Co^{2+}) = 3.87$ μ_B, $\mu_{\text{eff}}(Mn^{4+}) = 3.87$ μ_B. The calculated $\mu_{\text{eff}}^{\text{Theo}}$ (μ_B) values are 15.73 μ_B and 15.95 μ_B for HNMO and HCMO, respectively. It is worth noting that the values obtained from experiments are highly consistent with the theoretical predictions.

It is observed that there is a deviation in the paramagnetic region, indicated by the downturn in the χ^{-1} *vs.* T curve. This deviation is characteristic of the Griffiths phase that exists between the disordered paramagnetic phase and the ordered ferromagnetic phase. Both HNMO and HCMO compounds show the presence of the Griffiths phase. The evolution of such phase in Ho_2NiMnO_6 was reported by Bhatti *et al.*[29] and our previous work. The GP follows a power law,

$$\chi^{-1} = (T - T_C^R)^{1-\lambda} \quad (4)$$

where T_C^R is the random critical temperature and λ is the magnetic susceptibility exponent which lies between $0 \leq \lambda \leq 1$.[47,48] The double logarithmic plot of χ^{-1} *vs.* (T -T_C^R) is shown in Fig. 3(c and d) for HNMO and HCMO compounds. The exponent λ is a measure of the deviation from the Curie–Weiss law. The accurate choice of T_C^R is essential for the accurate determination of exponent λ. The value of T_C^R was found to be consistent, since T_C^R is recognized as the temperature for which fitting the data in the PM region yielded a λ value of nearly zero.[49] The λ_{GP} is estimated as 0.988 and 0.991 for HNMO and HCMO, respectively, while λ_{PM} is 0.064 and 0.005 from the linear portion of the curve at the applied magnetic field of 100 Oe. The larger values of λ_{GP} ($\sim$1) implies the Griffiths singularity.

The temperature-dependent magnetization M (H) curves with $\Delta T = 3$ K around their T_C with an applied magnetic field of 0–5 T for HNMO and HCMO are illustrated in Fig. 4(a and b). These M (H) data have been used to evaluate the magnetocaloric effect and the order of the magnetic phase transition. The magnetization curves show non-linear behavior, where, above T_C, linear behavior is observed, implying typical characteristics of ferromagnetic materials at finite temperatures due to thermal agitation disorienting the magnetic moments. The nature of the magnetic phase transition has been studied by analyzing the Arrott plots (M^2 *vs.* H/M) from M–H measurements, as shown in Fig. 4(c and d) for HNMO and HCMO compounds. According to Banerjee's criterion, a positive slope

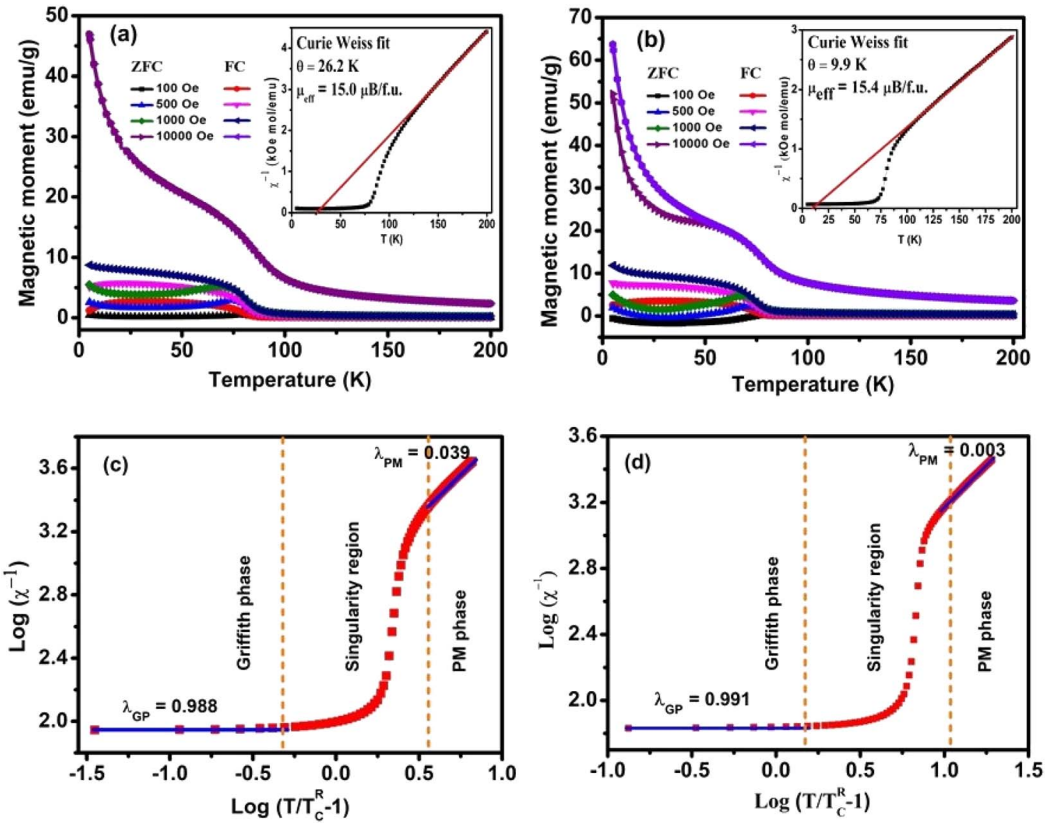

Fig. 3 (a and b) M–T FC-ZFC curves at various applied magnetic fields. Inset shows magnetic inverse susceptibility (χ^{-1}) as a function of temperature (T) under $H = 100$ Oe. Solid red line denotes Curie–Weiss fitting (C–W) for HNMO and HCMO compounds. (c and d) Log–log plot of χ^{-1} and $(T/T_C^R - 1)$ for inverse susceptibility measured at $H = 100$ Oe by following the eqn (4).

corresponds to the second-order magnetic transition, while a negative slope corresponds to the first-order magnetic transition.[50] From Fig. 4(a) and (b), the positive slopes without inflection in the low and high field regions are observed, indicating that the samples in the present study undergo the second order FM–PM phase transition.

The total entropy in a system consist of isothermal magnetic entropy (S_m), lattice entropy (S_{lat}), and electronic entropy (S_{ele}) and is given as,

$$S = S_m + S_{lat} + S_{ele} \quad (5)$$

The contributions of lattice and electronic entropy are considered to be negligible, hence, the total entropy can be approximated as the isothermal entropy change (ΔS), which can be estimated from the magnetization isotherms $M(H, T)$ shown in Fig. 4(a and b). Based on the thermodynamic theory, the isothermal field-induced magnetic entropy change (ΔS) from 0 to H_{max} can be calculated by using the relation:[12–15]

$$\Delta S(T,H) = S_M(T,H) - S_M(T,0) = \int_0^H \left(\frac{\partial s}{\partial H}\right)_T dH \quad (6)$$

The relationship between entropy and magnetization can be obtained by using the Maxwell equation $(\partial S/\partial H)_T = (\partial M/\partial T)_H$, then eqn (6) becomes,

$$\Delta S(T,H) = \int_0^H \left(\frac{\partial M}{\partial T}\right)_H dH \quad (7)$$

Fig. 5(a and b) shows the temperature dependence of magnetic entropy change (ΔS_M) calculated at different applied magnetic fields from 1 to 5 T for HNMO and HCMO compounds. Both compounds show similar behavior in MCE curve, $-\Delta S_M$ value reaches a maximum ΔS_{Max}, near the transition temperature (T_C) at low applied fields, and it increases with respect to H due to the improved ferromagnetic interactions. The calculated $-\Delta S_{Max}$ around 86 K, and 77 K are 1.7 and 2.2 J kg^{-1} K^{-1} for HNMO and HCMO samples, respectively, at $\Delta H = 0 - 5$ T. There might be a room for enhancement magnetocaloric properties at cryogenic temperatures, while it should be mentioned that the HNMO and HCMO samples in the present study are prepared by sol–gel method with nanocrystalline features. The magnetocaloric properties for studied HNMO and HCMO, along with other double perovskite compounds, are tabulated in Table 2. The comparison of $-\Delta S$ values shows significant difference in values for HNMO whereas, in the case of HCMO, it is increased slightly. The T_C values are different from our previous report as well as values reported by Chakraborty *et al.*[15] The differences in isothermal entropy change between studied samples with the literature is associated with the mass density, homogeneity, and quantitative relations

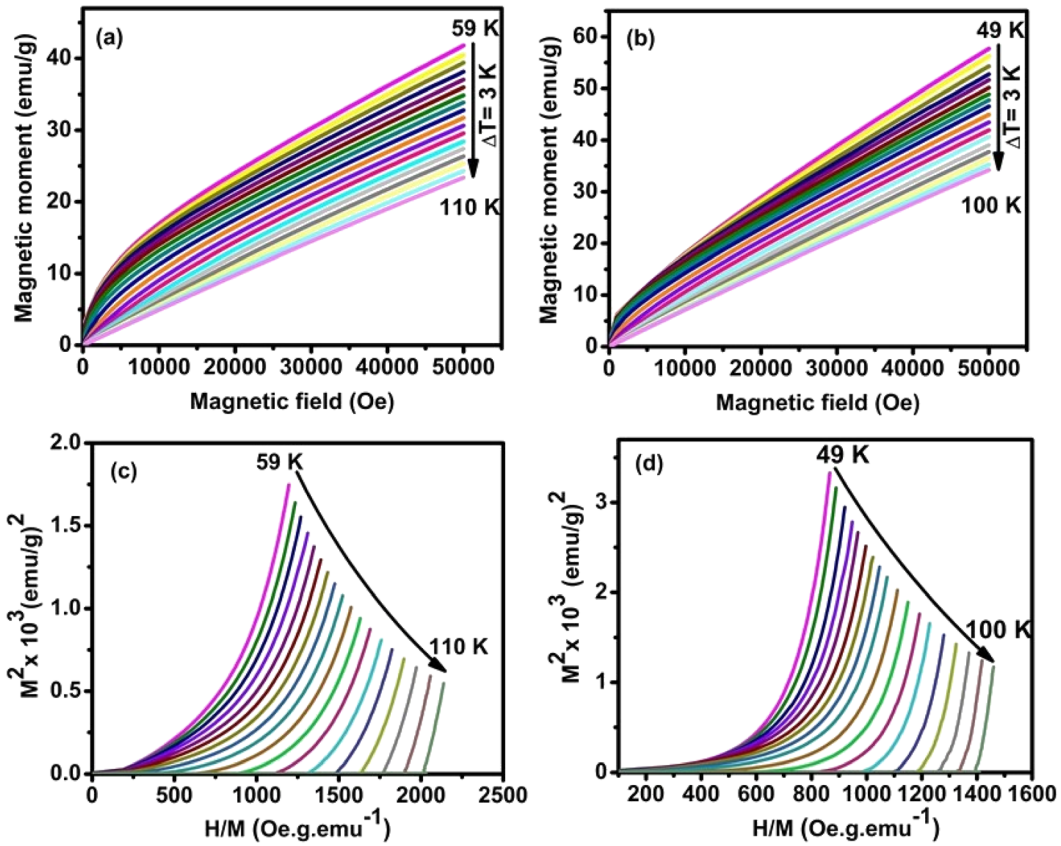

Fig. 4 (a–d) Isothermal magnetization curves and Arrot plots (M2 *vs.* *H*/*M*) at a various temperature in the vicinity of T_C with $\Delta T = 3$ K for HNMO and HCMO compounds.

between used reactants in the sample synthesis which are responsible for change in crystallite size and particle size. With decreasing crystallite size there is suppression of T_C, magnetization, and magnetic entropy change reported by Phan *et al.*[51] The shape of $-\Delta S$ curves is symmetric around T_C while it is not exactly symmetric in literature,[14] leading to the difference in $-\Delta S$ peak and $-\Delta S_{Max}$ values. The calculated values of $-\Delta S_{Max}$ are plotted as a function of H as shown in Fig. 6. It is clearly observed that ΔS_{Max} is proportional to an applied magnetic field.

Another method was used for crosscheck to determine the order of magnetic phase transitions. The field dependence of $-\Delta S$ of the sample is determined by utilizing the relation $\Delta S_{Max} = aH^n$, where a is constant and "n" is an exponent related to the

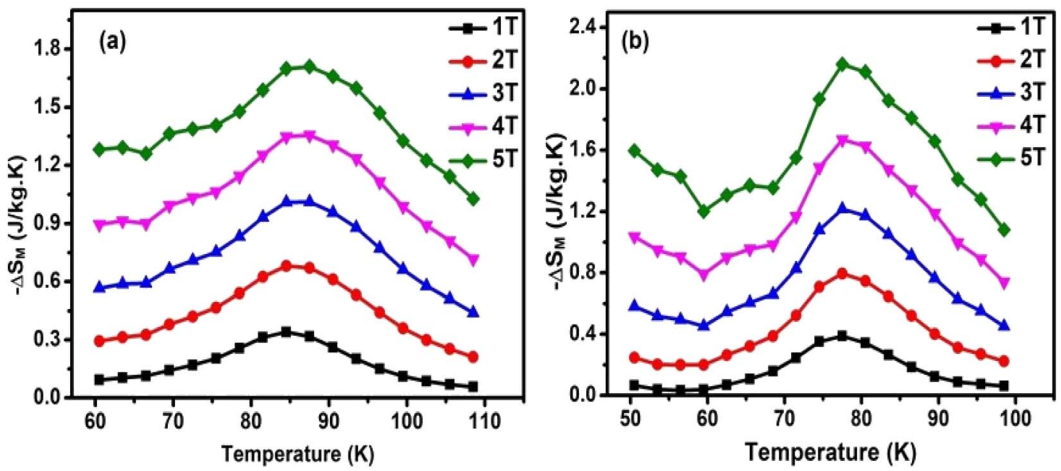

Fig. 5 Temperature dependence of magnetic entropy changes under different magnetic fields for (a) HNMO (b) HCMO compounds.

Table 2 ble 2Comparison of MCE properties of HNMO and HCMO with other rare earth based double perovskite compounds

Compound	T_C (K)	ΔH (T)	$-\Delta S_{Max}$ (J kg^{-1} K)	References
Ho_2NiMnO_6	81.2	5	1.7	Present
Ho_2CoMnO_6	73.5	5	2.2	Present
Ho_2NiMnO_6	71.5	5	3.1	32
Ho_2CoMnO_6	69	5	1.8	32
Ho_2NiMnO_6	86	5	6.4	15
Ho_2CoMnO_6	8	5	8.7	17
Nd_2NiMnO_6	156	5	2.9	33
Nd_2CoMnO_6	199	5	2.7	33
Pr_2NiMnO_6	208	7	3.15	24
Pr_2CoMnO_6	170	7	3.91	24
La_2NiMnO_6	260	3	0.98	56
La_2CoMnO_6	225	5	1.2	57
Eu_2NiMnO_6	143	5	3.2	13
Gd_2NiMnO_6	130	5	3.8	13
Tb_2NiMnO_6	112	5	3.5	13

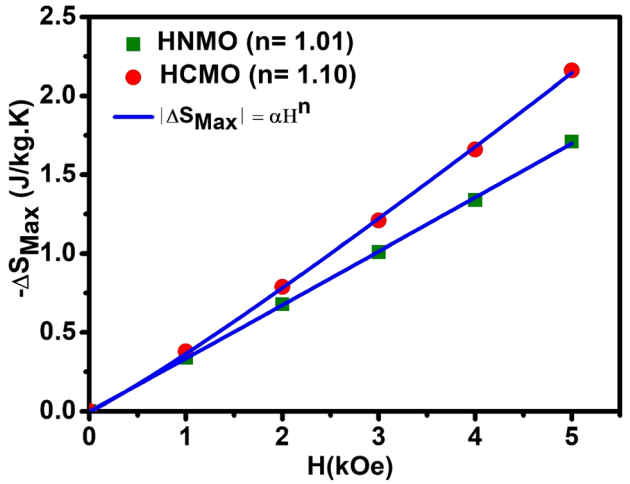

Fig. 6 The ΔS_{Max} values at a different magnetic field of HNMO and HCMO compounds fitted with a function $\Delta S_{Max} = \alpha \times H^n$, the values of exponent "n" are labeled in the figure.

magnetic order. Fig. 6 depicts – ΔS_{Max} with respect to the magnetic field along with power law fitting, and the resulting values of "n" are 1.01 and 1.10 for HNMO and HCMO compounds, respectively, which are higher than the reported values ($n = 0.67$) for mean field ferromagnetic materials.[12] The magnetic order can be analyzed from the equation $\Delta S_{Max} \propto H^n$, where the value of n depends on magnetic field and temperature, which can be calculated as follows:[52–55]

$$N(T,H) = \frac{d\ln|\Delta S(T,H)|}{d\ln(H)} \quad (8)$$

Fig. 7(a and b) shows temperature dependence of $N(T, H)$ at different magnetic field variation ΔH with 1, 2, 3, 4, and 5 T for HNMO and HCMO compounds. The overshoot of $N(T, H)$ value above 2 in case of HCMO compound at lower temperature region confirms the presence of FOMT in the compound along with SOMT while in case of HNMO compound $N(T, H)$ below the value 2 is confirming SOMT present in the compound. The shape of the $N(T, H)$ curves also indicates the FM–PM transition separated by the minimum around the Curie temperature. According to mean field theory (MFT), for long-range ferromagnet, at $T = T_C$, N tends to be the minimum value equal to 2/3 and $n = N(T_C)$, while it tends to be 1 and 2 as $T \ll T_C$ and $T \gg T_C$, respectively. The observed values of n near T_C are 1.03 and 1.15 for HNMO and HCMO, respectively, which are higher than MFT values, confirming the presence of the short-range magnetic order in these compounds. The experimentally determined values of n and $N(T, H)$ at $T = T_c$ suggest that both the HNMO and the HCMO experienced the second-order magnetic phase transition.

4. Conclusions

In summary, nanocrystalline double perovskite HNMO and HCMO were successfully synthesized by the sol–gel method. The Rietveld refinement revealed the formation of DP with space group $P2_1/n$, having a monoclinic crystal structure, along with the secondary phase of Ho_2O_3. The transmission electron

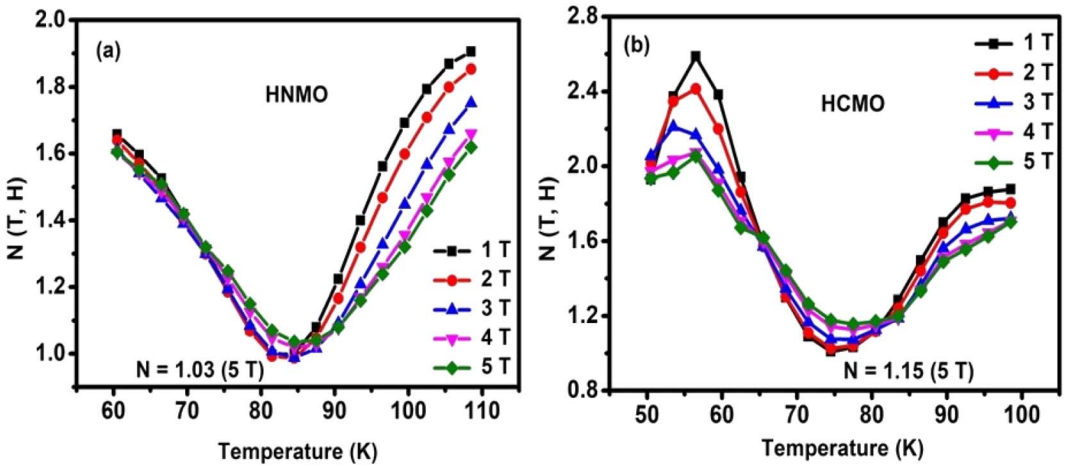

Fig. 7 Temperature dependence of $N(T, H)$ curves for (a) HNMO and (b) HCMO compounds at different magnetic field.

micrographs confirmed the formation of agglomerated nanocrystallites with particle size in the range of 50–200 nm. The calculated effective magnetic moments are consistent and close to theoretically predicted values. The downturn behavior in the inverse of magnetic susceptibility indicates the existence of the Griffiths phase, which has been further confirmed by the power law analysis. This feature arises in DP due to B-site lattice distortion, which originates from the smaller radius of the rare earth Ho atom. It is observed that both compounds show maximum MCE around T_C. The maximum values of $-\Delta S$ are 1.7 J kg^{-1} K^{-1} for Ho_2NiMnO_6 and 2.2 J kg^{-1} K^{-1} for Ho_2CoMnO_6 at $H = 50$ kOe. The Arrott plot confirms the second-order magnetic phase transition present in both compounds, also consistent with the analysis of magnetic order parameters n and N (T, H), implying the short-range magnetic order present in the studied compounds.

Conflicts of interest

There are no conflicts of interests to declare.

Acknowledgements

This work was supported by the Science Research Program through the National Research Foundation of Korea funded by the Ministry of Education, Science and Technology (NRF-2020R1I1A3070554) and Regional Innovation Strategy (RIS) through the National Research Foundation of Korea (2021RIS-004). Dr Y. Jo acknowledges the support by KBSI grant (No. 300200). Prof. D.-H. Kim would like to acknowledge the support by the Ministry of Science and ICT, (Project Number: (2022) ERIC02_2) and Commercialization Promotion Agency for R&D Outcomes (COMPA).

References

1 B. G. Shen, J. R. Sun, F. X. Hu, H. W. Zhang and Z. H. Cheng, Recent progress in exploring magnetocaloric materials, *Adv. Mater.*, 2009, **21**, 4545.
2 V. Franco, J. S. Blazquez, J. J. Ipus, J. Y. Law, L. Moreno-Ramirez and A. Conde, Magnetocaloric effect: from materials research to refrigeration devices, *Prog. Mater. Sci.*, 2017, **93**, 112.
3 L. W. Li, Review of magnetic properties and magnetocaloric effect in the intermetallic compounds of rare earth with low boiling point metals, *Chin. Phys. B*, 2016, **25**, 037502.
4 L. Li and M. Yan, Recent progresses in exploring the rare earth- based intermetallic compounds for cryogenic magnetic refrigeration, *J. Alloys Compd.*, 2020, **823**, 153810.
5 F. Z. Kassimi, H. Zaari, A. Benyoussef, A. Rachadi, M. Balli and A. E. Kenz, A theoretical study of the electronic, magnetic and magnetocaloric properties of the $TbMnO_3$ multiferroic, *J. Magn. Magn. Mater.*, 2022, **543**, 168397.
6 L. W. Li, Y. Yuan, Y. Qi, Q. Wang and S. Zhou, Achievement of a table-like magnetocaloric effect in the dual-phase ErZn/$ErZn_2$ composite, *Mater. Res. Lett.*, 2018, **6**, 67.
7 Y. K. Zhang, D. Guo, B. Wu, H. Wang, R. Guan, X. Li and Z. Ren, Magnetic properties, and magneto-caloric performances in RCo_2B_2C (R = Gd, Tb and Dy) compounds, *J. Alloys Compd.*, 2020, **817**, 152780.
8 Y. M. Wang, D. Guo, B. B. Wu, S. H. Geng and Y. K. Zhang, Magnetocaloric effect and refrigeration performance in $RE_{60}Co_{20}Ni_{20}$ (R = Ho and Er) amorphous ribbons, *J. Magn. Magn. Mater.*, 2020, **498**, 166179.
9 Y. Zhang, B. Wu, D. Guo, J. Wang and Z. Ren, Magnetic properties, and promising cryogenic magneto-caloric performances of $Gd_{20}Ho_{20}Tm_{20}Cu_{20}Ni_{20}$ amorphous ribbons, *Chin. Phys. B*, 2021, **30**, 017501.
10 K. Laajimi, M. Khlifi, E. K. Hlil, M. H. Gazzah and J. Dhahri, Enhancement of magnetocaloric effect by Nickel substitution in $La_{0.67}Ca_{0.33}Mn_{0.98}Ni_{0.2}O_3$ manganite oxide, *J. Magn. Magn. Mater.*, 2019, **491**, 165625.
11 T. L. Phan, N. T. Dang, T. A. Ho, J. S. Rhyee, W. H. Shon, K. Tarigan and T. V. Manh, Magnetic and magnetocaloric properties of $Sm_{1-x}Ca_xMnO_3$ (x = 0.88) nanoparticles, *J. Magn. Magn. Mater.*, 2017, **443**, 233.
12 K. P. Shinde, E. J. Lee, M. Manawan, A. Lee, S.-Y. Park, Y. Jo, K. Ku, J. M. Kim and J. S. Park, Structural, magnetic, and magnetocaloric properties of R_2NiMnO_6 (R = Eu, Gd, Tb), *Sci. Rep.*, 2021, **11**, 20206.
13 I. N. Bhatti, I. N. Bhatti, R. N. Mahato and M. A. H. Ahsan, Physical properties in nanocrystalline Ho_2CoMnO_6, *Ceram. Int.*, 2020, **46**, 46.
14 J. Y. Moon, M. K. Kim, Y. J. Choi and N. Lee, Giant Anisotropic Magnetocaloric Effect in Double-perovskite Gd_2CoMnO_6 Single Crystals, *Sci. Rep.*, 2017, **7**, 16099.
15 T. Chakraborty, H. Nhalil, R. Yadav, A. A. Wagh and S. Elizabeth, Magnetocaloric properties of R_2NiMnO_6 (R=Pr, Nd, Tb, Ho and Y) double perovskite family, *J. Magn. Magn. Mater.*, 2017, **428**, 59.
16 L. Li, P. Xu, S. Ye, Y. Li, G. Liu, D. Huo and M. Yan, Magnetic properties and excellent cryogenic magnetocaloric performances in B-site ordered RE_2ZnMnO_6 (RE = Gd, Dy and Ho) perovskites, *Acta Mater.*, 2020, **194**, 354.
17 Y. Jia, Q. Wang, P. Wang and L. Li, Structural, magnetic and magnetocaloric properties in R_2CoMnO_6 (R = Dy, Ho, and Er), *Ceram. Int.*, 2017, **43**, 15856.
18 L. Li and M. Yan, Recent progress in the magnetic and cryogenic magnetocaloric properties of $RE_2TMTM'O_6$ double perovskite oxides, *J. Mater. Sci. Technol.*, 2023, **136**, 1.
19 R. Das, R. Prabhu, N. Venkataramani, S. Prasad, L. Li, M.-H. Phan, V. Keppens, D. Mandrus and H. Srikanth, Giant low-field magnetocaloric effect and refrigerant capacity in reduced dimensionality EuTiO3 multiferroics, *J. Alloys Compd.*, 2021, **850**, 156819.
20 M. Balli, B. Roberge, P. Fournier and S. Jandl, Review of the Magnetocaloric Effect in $RMnO_3$ and RMn_2O_5 Multiferroic Crystals, *Crystals*, 2017, **7**, 44.
21 M.-H. Phan and S.-C. Yu, Review of the magnetocaloric effect in manganite materials, *J. Magn. Magn. Mater.*, 2007, **308**, 325.
22 B. Wu, D. Guo, Y. Wang and Y. Zhang, Crystal structure, magnetic properties, and magnetocaloric effect in B-site

disordered RE_2CrMnO_6 (RE = Ho and Er) perovskites, *Ceram. Int.*, 2020, **46**, 11988.

23 A. Pal, P. Singh, V. Gangwar, S. Ghosh, P. Prakash, S. Saha, A. Das, M. Kumar, A. Ghosh and S. Chatterjee, B-site disordered driven multiple-magnetic phase: Griffiths phase, re-entrant cluster glass, and exchange bias in Pr_2CoFeO_6, *Appl. Phys. Lett.*, 2019, **114**, 252403.

24 A. Hossain, P. Bandyopadhyay and S. Roy, An overview of double perovskites $A_2BB'O_6$ with small ions at A site: Synthesis, structure, and magnetic properties, *J. Alloys Compd.*, 2018, **740**, 414.

25 S. Ivanov, M. Andersson, J. Cedervall, E. Lewin, M. Sahlberg, G. Bazuev, P. Nordblad, R. S. I. Mathieu, M. Andersson, J. Cedervall, E. Lewin, M. Sahlberg, G. Bazuev, P. Nordblad and R. Mathieu, Temperature-dependent structural and magnetic properties of R_2MMnO_6 double perovskites (R = Dy, Gd; M = Ni, Co), *J. Mater. Sci.: Mater. Electron.*, 2018, **29**, 18581.

26 Z. Q. Zhang, P. Xu, Y. S. Jia and L. W. Li, Structural, magnetic and magnetocaloric properties in distorted RE_2NiTiO_6 double perovskite compounds, *JPhys Energy*, 2023, **5**, 014017.

27 M. Balli, S. Mansouri, P. Fournier, S. Jandl, K. D. Truong, S. Khadechi-Haj Khlifa, P. de Rango, D. Fruchart and A. Kedous-Lebouc, Enlarging the magnetocaloric operating window of the Dy_2NiMnO_6 double perovskite by lanthanum doping, *J. Phys. D: Appl. Phys.*, 2020, **53**, 095001.

28 J. B. Goodenough, *Magnetism and the Chemical Bond*, Inter-Science, New York, 1976.

29 I. N. Bhatti, I. N. Bhatti, R. N. Mahato and M. A. H. Ahsan, Griffiths phase and magneto-transport study in 3d based nanocrystalline double perovskite Pr_2CoMnO_6, *Phys. Lett. A*, 2019, **383**, 2326.

30 J. K. Murthy, K. D. Chandrasekhar, S. Mahana and D. Topwal, Giant magnetocaloric effect in Gd_2NiMnO_6 and Gd_2CoMnO_6 ferromagnetic insulators, *J. Phys. D: Appl. Phys.*, 2015, **48**, 355001.

31 Y. Zhang, H. Li, D. Guo, L. Hou, X. Li, Z. Ren and G. Wilde, Cryogenic magnetic properties and magnetocaloric performance in double perovskite Pr_2NiMnO_6 and Pr_2CoMnO_6 compounds, *Ceram. Int.*, 2018, **44**, 20762.

32 K. P. Shinde, M. Manawan, S.-Y. Park, Y. Jo, V. M. Tien, Y. Pham, S.-C. Yu, N. Kalanda, M. Yarmolich, A. Petrov and D.-H. Kim, Structural, magnetic and magnetocaloric properties of double perovskite Ho_2MMnO_6 (M = Fe, Co, and Ni), *J. Magn. Magn. Mater.*, 2022, **544**, 168666.

33 Y. Li, Q. Lv, S. Feng, K. M. Rehman, X. Kan and X. Liu, A comparative investigation of B-site ordering and structure, magnetic, magnetocaloric effect, critical behavior in double perovskite Nd_2BMnO_6 (B = Co and Ni), *Ceram. Int.*, 2021, **47**, 32599.

34 M. Cernea, F. Vasiliu, C. Plapcianu, C. Bartha, I. Mercioniu, I. Pasuk, R. Lowndes, R. Trusca, G. V. Aldica and L. Pintilie, Preparation by sol–gel and solid state reaction methods and properties investigation of double perovskite Sr_2FeMoO_6, *J. Eur. Ceram. Soc.*, 2013, **33**, 2483.

35 Z. Q. Zhang, P. Xu, Y. S. Jia and L. W. Li, Structural, magnetic and magnetocaloric properties in distorted RE_2NiTiO_6 double perovskite compounds, *JPhys Energy*, 2023, **5**, 014017.

36 S. S. Zheng, C. L. Li, C. X. Bai, K. X. Zhou, P. Wang, Y. Lu, Y. Qiu and Y. S. Luo, Magnetic properties and enhanced cryogenic magnetocaloric effect in Ti-substituted Gd_2CoMnO_6 double perovskites, *J. Magn. Magn. Mater.*, 2022, **564**, 170162.

37 K. Pushpanjali Patra and S. Ravi, Re-entrant Spin Glass and Magnetocaloric Effect in Frustrated Double Perovskite Ho_2CoMnO_6 Flat Nanorod, *J. Magn. Magn. Mater.*, 2022, **559**, 69537.

38 A. A. Coelho, TOPAS and TOPAS-Academic: An optimization program integrating computer algebra and crystallographic objects written in C++, *J. Appl. Crystallogr.*, 2018, **51**, 210.

39 K. Momma and F. Izumi, VESTA 3 for three-dimensional visualization of crystal, volumetric and morphology data, *J. Appl. Crystallogr.*, 2011, **44**, 1272.

40 T. Chakraborty, H. S. Nair, H. Nhalil, K. R. Kumar, A. M. Strydom and S. Elizabeth, Disordered ferromagnetism in Ho_2NiMnO_6 double perovskite, *J. Phys.: Condens. Matter*, 2017, **29**, 025804.

41 Y. S. Jia, Q. Wang, Y. Qi and L. W. Li, Multiple magnetic phase transitions and magnetocaloric effect in double perovskites R_2NiMnO_6 (R = Dy, Ho, and Er), *J. Alloys Compd.*, 2017, **726**, 1132.

42 Y. Zhang, B. Zhang, S. Li, J. Zhu, B. Wu, J. Wang and Z. Ren, Cryogenic magnetic properties and magnetocaloric effects (MCE) in B-site disordered RE_2CuMnO_6 (RE = Gd, Dy, Ho and Er) double perovskites (DP) compounds, *Ceram. Int.*, 2021, **47**, 18205.

43 S. Vasala and M. Karppinen, $A_2B'B''O_6$ perovskites: a review, *Prog. Solid State Chem.*, 2015, **43**, 1.

44 W. Z. Yang, X. Q. Liu, H. J. Zhao, Y. Q. Lin and X. M. Chen, Structure, magnetic, and dielectric characteristics of Ln_2NiMnO_6 (Ln = Nd and Sm) ceramics, *J. Appl. Phys.*, 2012, **112**, 064104.

45 D. Kumar, P. Jena and A. K. Sing, Structural, magnetic, and dielectric studies on half-doped $Nd_{0.5}Ba_{0.5}CoO_3$ perovskite, *J. Magn. Magn. Mater.*, 2020, **516**, 167330.

46 M. Retuerto, A. Munoz, M. J. Martinez-Lope, J. A. Alonso, F. J. Mompean, M. T. Fernandez-Diaz and J. Sanchez-Benitez, Magnetic interactions in the double perovskites R2NiMnO6 (R = Tb, Ho, Er, Tm) investigated by neutron diffraction, *Inorg. Chem.*, 2015, **54**, 10890.

47 R. B. Griffiths, Nonanalytic behavior above the critical point in a random Ising ferromagnet, *Phys. Rev. Lett.*, 1969, **23**, 17.

48 K. Anand, M. Alam, A. Pal, P. Singh, S. Kumari, A. G. Joshi, A. Das, A. Mohan and S. Chatterjee, Existence of Griffiths phase and unusual spin dynamics in double perovskite Tb_2CoMnO_6, *J. Magn. Magn. Mater.*, 2021, **528**, 167697.

49 S. Karmakar, S. Majumdar, T. K. Nath and S. Giri, Observation of Griffiths phase in antiferromagnetic $La_{0.32}Eu_{0.68}MnO_3$, *J. Phys.: Condens. Matter*, 2012, **24**, 126003.

50 S. K. Banerjee, On a generalised approach to first and second order magnetic transitions, *Phys. Lett.*, 1964, **12**, 16.

51 T. L. Phan, T. D. Thanh, P. Zhang, D. S. Yang and S. C. Yu, The magnetic phase transition and magnetocaloric effect in $Sm_{0.58}Sr_{0.42}MnO_3$ nanoparticles, *Solid State Commun.*, 2013, **166**, 32.

52 V. Franco, J. S. Blázquez, J. J. Ipus, J. Y. Law, L. M. Moreno-Ramírez and A. Conde, Magnetocaloric effect: From materials research to refrigeration devices, *Prog. Mater. Sci.*, 2017, **93**, 112.

53 Y. Zhang, Y. Tian, Z. Zhang, Y. Jia, B. Zhang, M. Jiang, J. Wang and Z. Ren, Magnetic properties and giant cryogenic magnetocaloric effect in B-site ordered antiferromagnetic Gd_2MgTiO_6 double perovskite oxide, *Acta Mater.*, 2022, **226**, 117669.

54 Y. Zhang, J. Zhu, S. Li, Z. Zhang, J. Wang and Z. Ren, Magnetic properties and promising magnetocaloric performances in the antiferromagnetic $GdFe_2Si_2$ compound, *Sci. China Mater.*, 2022, **65**, 1345.

55 D. Guo, L. M. Moreno-Ramírez, C. Romero-Muñiz, Y. Zhang, J. Y. Law, V. Franco, J. Wang and Z. Ren, First- and second-order phase transitions in RE_6Co_2Ga (RE = Ho, Dy or Gd) cryogenic magnetocaloric materials, *Sci. China Mater.*, 2021, **64**, 2846.

56 T. V. Manh, T. A. Ho, T. D. Thanh, T. L. Phan, M. H. Phan and S. Yu, Critical Behavior and Magnetocaloric effect in La_2NiMnO_6 Nanocrystals, *IEEE Trans. Magn.*, 2015, **51**, 1.

57 M. Balli, P. Fournier, S. Jandl, K. D. Truong and M. M. Gospodinov, Analysis of the phase transition and magneto-thermal properties in La_2CoMnO_6 single crystals, *J. Appl. Phys.*, 2014, **116**, 073907.